Chinese Chemical Letters 34 (2023) 108242

Contents lists available at ScienceDirect

Chinese Chemical Letters

journal homepage: www.elsevier.com/locate/cclet

Molecular dynamics simulations of the Li-ion diffusion in the amorphous solid electrolyte interphase

Jianxin Tian[a,b], Taiping Hu[c], Shenzhen Xu[c,*], Rui Wen[a,b,*]

[a] CAS Key Laboratory of Molecular Nanostructure and Nanotechnology, CAS Research/Education Center for Excellence in Molecular Sciences, Beijing National Laboratory for Molecular Science (BNLMS), Institute of Chemistry, Chinese Academy of Sciences, Beijing 100190, China
[b] University of Chinese Academy of Sciences, Beijing 100049, China
[c] School of Materials Science and Engineering, Peking University, Beijing 100871, China

ARTICLE INFO

Article history:
Received 15 December 2022
Revised 11 January 2023
Accepted 16 February 2023
Available online 19 February 2023

Keywords:
Molecular dynamics
Amorphous solid electrolyte interphase
Li-ion diffusion

ABSTRACT

The solid electrolyte interphase (SEI), a passivation film covering the electrode surface, is crucial to the lifetime and efficiency of the lithium-ion (Li-ion) battery. Understanding the Li-ion diffusion mechanism within possible components in the mosaic-structured SEI is an essential step to improve the Li-ion conductivity and thus the battery performance. Here, we investigate the Li-ion diffusion mechanism within three amorphous SEI components (*i.e.*, the inorganic inner layer, organic outer layer, and their mixture with 1:1 molar ratio) *via ab initio* molecular dynamic (AIMD) simulations. Our simulations show that the Li-ion diffusion coefficient in the inorganic layer is two orders of magnitude faster than that in the organic layer. Therefore, the inorganic layer makes a major contribution to the Li-ion diffusion. Furthermore, we find that the Li-ion diffusivity in the organic layer decreases slightly with the increase of the carbon chain from the methyl to ethyl owing to the steric hindrance induced by large groups. Overall, our current work unravels the Li-ion diffusion mechanism, and provides an atomic-scale insight for the understanding of the Li-ion transport in the SEI components.

Rechargeable Li-ion batteries (LIBs) have been widely used in critical applications such as portable electronics, heavy-duty vehicles, and medical equipment due to their high energy storage [1–6]. However, as the global energy demand continues to grow, it becomes increasingly important to develop energy storage systems with higher energy densities. Solid electrolyte interphase (SEI) or cathode electrolyte interphase (CEI) is constructed from the side reactions such as electrolyte decomposition on the electrode's surface during the first charge and discharge of Li-ion batteries [7]. Although this layer of SEI/CEI would lead to irreversible loss of battery capacity in the first cycle, a good SEI or CEI layer should prevent further electrolyte decomposition by blocking the electron transport while allowing the Li-ion to pass through during long cycling, thus ensuring good cycling performance of the battery [8–12]. Meanwhile, the composition, thickness, morphology, and compactness of SEI/CEI significantly affect battery performance [13–15]. Therefore, understanding the Li-ion transport properties of the solid electrolyte interphase is critical for designing long-life and high-performance batteries.

Tremendous research has provided a complete picture of SEI film chemistry and a general understanding of the mechanism of its formation [16,17]. The composition of SEI/CEI films has been revealed by researchers, mainly consisting of the inorganic components (*e.g.*, Li_2CO_3, LiF and Li_2O) near the electrodes and the organic components (*e.g.*, $ROCO_2Li$, ROLi (R is an organic group)) near the electrolyte through *in situ* and *ex situ* compositional characterization techniques [18,19]. The morphological aspects of the SEI/CEI evolution process and thickness have been proposed with scanning electron microscopy (SEM), transmission electron microscopy (TEM), and atomic force microscopy (AFM) [20–22]. However, the Li-ion transport mechanism passing through the SEI and understanding of ionic conductivity are still under debate [23,24]. Several computational studies developed independently defect thermodynamics and diffusion mechanisms of SEI in inorganic crystal components, organic components such as dilithium ethylene dicarbonate (Li_2EDC) and dilithium butylene dicarbonate (Li_2BDC), and the grain boundary [25–28]. One of the currently accepted SEIs is the mosaic structure, that is, a dispersion of crystalline phases in these amorphous phases and its random distribution will cause more cracks and other problems during the cycles [29,30]. However, relatively little attention has been paid to understanding the Li-ion transport mechanism in the amorphous structures [31].

* Corresponding authors.
E-mail addresses: xushenzhen@pku.edu.cn (S. Xu), ruiwen@iccas.ac.cn (R. Wen).

https://doi.org/10.1016/j.cclet.2023.108242
1001-8417/

Therefore, it is necessary to understand the Li-ion transport in the amorphous solid electrolyte interphase.

Molecular dynamics simulations are widely used to estimate diffusion behavior because it provides dynamic information about the system's evolution concerning time [32–34]. Here, the migration of the Li-ion in the SEI/CEI was investigated through *ab initio* molecular dynamics (AIMD) simulations. Three amorphous solid electrolyte interphases were constructed namely the inorganic inner layer of LiF and Li_2CO_3, the organic outer layer of $ROCO_2Li$ and ROLi (R = CH_3 or CH_3-CH_2), and the mixing layer of their 1:1 mixture. Room-temperature diffusivities in different components are obtained using the Arrhenius extrapolation relationship. Furthermore, the effect of the carbon chain length on the Li-ion diffusion in the organic layer is revealed. Our work elucidates the Li-ion diffusion mechanism in different amorphous SEI components and provides guides for SEI optimization with enhanced Li-ion conductivity for battery designs.

In order to study the diffusion of Li-ion in three amorphous solid electrolyte interphases of the inorganic, organic, and mixing layers, we have performed density functional theory (DFT) calculations using the Vienna *ab initio* Simulation Package (VASP) [35–37]. The projector augmented wave (PAW) method [38] and Perdew-Burke-Ernzerhof (PBE) [39] functional were used throughout the work. The kinetic cutoff energy was 500 eV and GAMMA-centered k-point meth was used for all calculations, determined by the convergence tests.

The calculation and simulation are mainly carried out in the following three parts: (1) Structural relaxation: to eliminate the unreasonable contacts in the initially setup amorphous structures; (2) 10 ps *NpT* ensemble: AIMD simulation with an *NpT* ensemble at 300 K was performed to obtain the equilibrium volume of 300 K, *i.e.*, the reasonable density of these different components in SEI. The Langevin thermostat was used to run an *NpT* simulation [40,41]; (3) 100 ps *NVT* ensemble: A range of high temperatures (600, 700, 800, 900, 1000, 1100, 1200 and 1500 K) with *NVT* ensembles were performed for the sampling and extrapolating to the room-temperature diffusivity. The 1 fs time step and the Nose-Hoover thermostat were used in all *NVT* simulations [42,43].

The gradient amorphous and crystalline phase components of SEI affect the internal Li-ion transport. Numerous studies have found the presence of amorphous interphases on the cathode and anode surfaces, which exerts a significant influence on the electrochemical behavior [20,44]. Therefore, we constructed the following three types of amorphous SEI components, namely, the inorganic layer of the LiF and the Li_2CO_3, the organic layer of the $ROCO_2Li$ and the ROLi (R = CH_3 or CH_3-CH_2), and their mixing layer with 1:1 ratio, to compare the effects of the organic and inorganic components on the Li-ion migration, using the DFT method to calculate the energy and force of the system (Fig. 1).

To construct the amorphous solid electrolyte interphase, we used the Packmol software [45] to build the inorganic, organic, and mixing layers, consisting of 15 Li_2CO_3 and LiF, 8 CH_3OLi and CH_3OCO_2Li, and 6 Li_2CO_3, LiF, CH_3OLi and CH_3OCO_2Li molecules, with a total of 120, 120, and 138 atoms, respectively, based on the cost and computational time limit of AIMD. The initial box shapes are $14 \times 14 \times 14$ Å^3, $13 \times 13 \times 13$ Å^3, and $18 \times 18 \times 18$ Å^3, as shown in Fig. S1 (Supporting information). Similarly, the carbon chain is increased to an ethyl configuration, containing 6 CH_3CH_2OLi and $CH_3CH_2OCO_2Li$, totaling 126 atoms, and then stacked in a $15 \times 15 \times 15$ Å^3 cubic simulation box (Fig. S1c). The Li, F and CO_3 groups are randomly placed into a box with periodic boundaries and the bond length and bond angle of the CO_3^{2-} group are derived from the inorganic crystal structure database (ICSD).

The final amorphous morphologies are obtained according to the steps mentioned above, as shown in Figs. S1a'-d'. The final sizes of the boxes are $11.07 \times 11.07 \times 11.07$ Å^3, $11.54 \times 1.54 \times 1.54$ Å^3, $11.61 \times 11.61 \times 11.61$ Å^3, $12.34 \times 12.34 \times 12.34$ Å^3 for the inorganic layer, the methyl organic layer, the ethyl organic layer, and the mixing layer, respectively. The atomic groups diffuse uniformly and C-O and C-C bonds do not cleavage. As the MD simulation progresses, changes in temperature and energy in each system are monitored to ensure that the simulation reaches equilibrium. Fig. S2 (Supporting information) shows the apparent temperature and energy changes obtained at different temperatures, essentially in equilibrium after 5 ps.

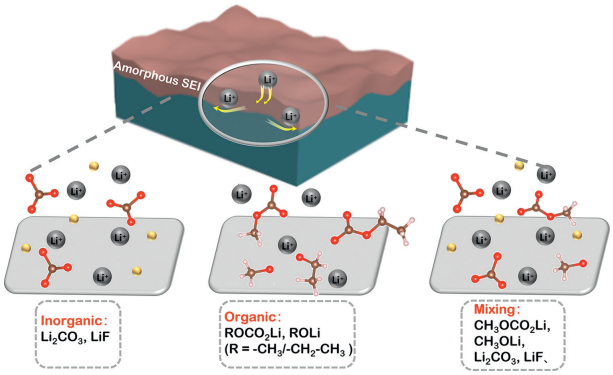

Fig. 1. Schematic diagram of Li-ion diffusion in the amorphous SEI regions with different components.

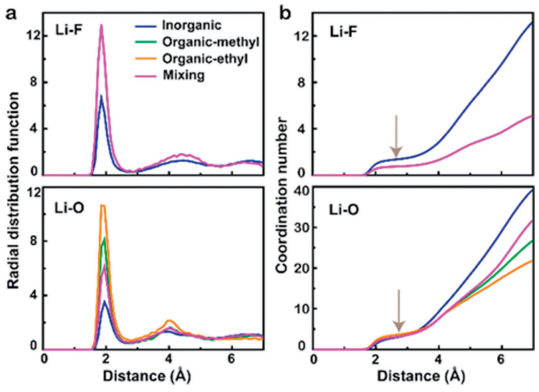

Fig. 2. (a) Radial distribution functions and (b) coordination numbers for the inorganic layer, the methyl organic layer, the ethyl organic layer, and the mixing layer at 600 K. The arrows indicate the first coordination shell: 2.65 Å for Li-F and ~2.75 Å for Li-O.

The amorphous SEI structures are analyzed by examining radial distribution functions (RDFs) involving F and O, which are compared among systems with different compositions (Fig. 2). The higher Li-F RDF peak in the mixing system (Fig. 2a) corresponds to a relatively smaller coordination number (Fig. 2b) compared to the inorganic component system because the average densities of the calculated group in different compositional SEI layers are different. The Li-F first peak is around 1.85 Å. The Li-F peaks are located at the same distances of 1.85 Å in different components. The Li^+ ion is strongly coordinated by the F^- ions in the inorganic layer as opposed to the mixing layer, with coordination numbers of 1.36 fluorine atoms in the inorganic layer and 0.75 fluorine atoms in the mixing layer within a distance of 2.65 Å to a Li^+ ion. The choice of the Li-F coordination number sheath of 2.65 Å depends on the distance where the Li-F RDF decays to the first valley, so fluorine within 2.65 Å is considered to be strongly coordinating with the Li^+ ion. The position of the first peak of the Li-O RDF is around 1.95 Å for all systems. Even though the interaction between Li/F restricts the movement of ions, it still has a similar Li-O coordination shell of ~2.75 Å, indicating that the Li^+ ion is surrounded

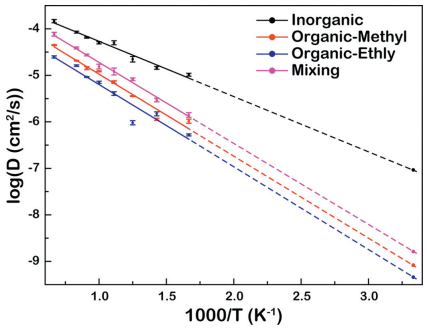

Fig. 3. Linear fitting of log(*D*)-1000/*T* of the inorganic layer, organic layer (methyl, ethyl) and mixing layer.

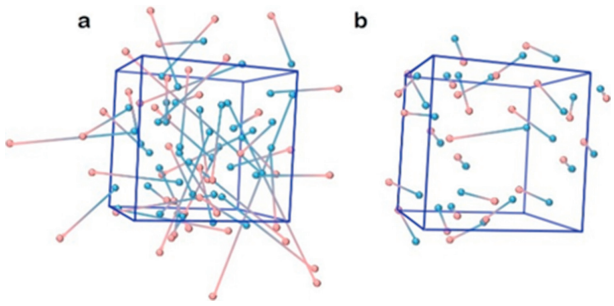

Fig. 4. Displacements of the Li-ion for (a) the inorganic layer and (b) the methyl-organic layer at 600 K.

by another three to four O atoms in the coordination sheath. Due to the higher proportion of O atoms in the organic components, the corresponding first solvation sheath (2.85 Å) is larger and has more oxygen coordination atoms (3.80) (Fig. S3 in Supporting information).

We study the Li-ion transport in the SEI by calculating Li-ion self-diffusion coefficients (D_s) by the mean square displacement over time in different compositional layers:

$$D_s = \lim_{t\to\infty}\left[\frac{1}{2dt}\left\langle[\vec{r}(t)]^2\right\rangle\right] \quad (1)$$

where *d* indicates the Li diffusion dimension and it equals 3 in our cases. The $\langle[\vec{r}(t)]^2\rangle$, that is MSD(*t*), is a mean-square displacement of all Li-ions during time *t*, calculated according to the following formula:

$$\left\langle[\vec{r}(t)]^2\right\rangle = \frac{1}{N}\sum_i^N\left\langle[\vec{r}(t+t_0)]^2 - [\vec{r}_t(t_0)]^2\right\rangle \quad (2)$$

MSD is the average overall Li-ions of *N* and is a statistical average over time t_0. Speaking generally, a sufficient sampling at room temperature requires a long time (> 10 ns) simulation, which goes far beyond the time scale of the AIMD. Therefore, the Arrhenius relationship was used to extrapolate the room-temperature diffusion coefficient from the high-temperature results [46,47].

To investigate the ionic diffusivity, the MSDs of the Li-ion in the SEI layer at different temperatures were calculated (Fig. S4a in Supporting information). The overall MSD at each temperature was obtained from the three directions *a*, *b* and *c* (Fig. S4b in Supporting information). As shown, the MSD of the Li-ion increases almost linearly with time, indicating that sampling is sufficient and the diffusion is relatively uniform [48]. At the same time, it can be seen that the diffusion coefficient increases with the increase in temperature because the high temperature intensifies the movement and collision of molecules, which is beneficial to diffusion. The slope of the MSD curves is used to calculate the diffusion coefficient by Eq. 1. Owing to the poor statistics, the first and last 10% MSD curves are excluded to linearly fit the diffusivity and the final results are listed in Tables S1-S4 (Supporting information) [49].

Both the Li-ion diffusion coefficient and ionic conductivity were extracted from the slopes of the MSD linear fitting and then extrapolated to low temperatures. Based on the above MSD curves, the Arrhenius plot log(*D*)-1000/*T* of the diffusion coefficient from 600 K to 1500 K are shown in Fig. 3, including the inorganic layer, the methyl organic layer, the ethyl organic layer, and the mixing layer. The corresponding calculation data are recorded in Tables S5-S8 (Supporting information). It can be seen that as the temperature decreases, the Li-ion diffusion coefficient in the inorganic layer decreases more slowly than that of the organic layer, which indicates that the Li-ion is more mobile in the inorganic small molecules at low temperatures. Therefore, the Li-ion diffusion coefficient of 9.24×10^{-8} cm^2/s in the inorganic layer extrapolated to room temperature of 300 K was found to be two orders of magnitude larger than the diffusion in the methyl-organic layer of 8.29×10^{-10} cm^2/s and at least an order of magnitude larger than the Li-ion diffusion of 1.63×10^{-9} cm^2/s in the mixing layer (Table S9 in Supporting information). Although bulk LiF is an electronic insulator, numerous studies have proved that LiF-rich SEI (polycrystalline and amorphous LiF) has a great advantage in Li-ion transport when forming nanoscale interfaces with other components (Li_2O, Li_2CO_3), which may be that they synergistically form a heterogeneous structure, improving the ionic conductivity on the anode side of the battery, and also consistent with our AIMD simulations [50,51]. At first glance, the Li-ion diffusion coefficients of the two sizes of organic group layers are in the same order of magnitude, but the methyl organic layer is slightly larger, which also indicates that the large group formed by the increase of the carbon chain does restrict the Li-ion diffusion. The activation energy of the Li-ion diffusion can be calculated using the Arrhenius formula. The results show that the Li-ion has smaller activation energy in the inorganic layer, indicating a faster diffusion coefficient, which is consistent with our previous calculations.

In order to gain further insights into the transport mechanism of the Li-ion in different SEI components, the trajectories after 5 ps where the system reaches equilibrium are selected for analysis. Fig. 4 shows the displacement of the Li-ion over 5 ps, where blue and pink balls represent the initial and final positions of the Li-ion during the simulation segment, respectively, and the arrows indicate the directions of each Li-ion's movement. It can be seen that in the inorganic SEI component, after the 100 ps AIMD simulation, the range of Li-ion movement is larger. This visualized schematic diagram of the Li-ion diffusion is consistent with the calculated Li-ion mobility, which once again proves the binding effect of organic components. In the future design of battery performance, it should be considered to preferentially induce the formation of inorganic-rich components SEI, to effectively improve the Li-ion diffusion in the interphases.

In summary, AIMD simulations are performed to investigate the Li-ion diffusion coefficient and ionic conductivity for different amorphous SEI components. Furthermore, the Li-ion transport mechanism in those components is revealed. Our simulations show that the Li-ion diffusion in the inorganic layer is significantly faster than that in the organic layer, while the diffusion in the mixing layer is between the two. Meanwhile, as the carbon chain increases from methyl to ethyl in the organic layer, the Li-ion diffusion is limited and a slightly lower diffusion coefficient is obtained. This effect is related to the group size of the $ROCO_2^-$ anions, which limits the Li-ion diffusion in the interphases, thereby reducing the Li-ion conductivity. Overall, our current work provides an understanding of the Li-ion transport mechanism in the amorphous SEI at the atomic scale and provides the guidance for the battery interphase design.

Declaration of competing interest

The authors declare that they have no known competing financial interests or personal relationships that could have appeared to influence the work reported in this paper.

Acknowledgments

R. Wen acknowledges the financial support from the National Key R&D Program of China (No. 2021YFB2500300) and the CAS Project for Young Scientists in Basic Research (No. YSBR-058). S. Xu acknowledges funding support from the Chinese Ministry of Science and Technology (No. 2021YFB3800303), DP Technology Corporation (No. 2021110016001141), and the School of Materials Science and Engineering at Peking University.

Supplementary materials

Supplementary material associated with this article can be found in the online version at doi:10.1016/j.cclet.2023.108242.

References

[1] M. Armand, J.M. Tarascon, Nature 451 (2008) 652–657.
[2] B. Kang, G. Ceder, Nature 458 (2009) 190–193.
[3] B. Dunn, H. Kamath, J.M. Tarascon, Science 334 (2011) 928–935.
[4] V. Etacheri, R. Marom, R. Elazari, et al., Energy Environ. Sci. 4 (2011) 3243–3262.
[5] S.C. Zhang, S.Y. Li, Y.Y. Lu, eScience 1 (2021) 163–177.
[6] T. Xu, C.K. Zhou, H.H. Zhou, et al., Chin. J. Chem. 37 (2019) 342–346.
[7] Z.Q. Rong, D. Kitchaev, P. Canepa, W.X. Huang, G. Ceder, J. Chem. Phys. 145 (2016) 074112.
[8] X.B. Cheng, Y. Chong, X.Q. Zhang, L. He, Z. Qiang, ACS Energy Lett. 3 (2018) 1564–1570.
[9] Y.F. Su, G. Chen, L. Chen, et al., Chin. J. Chem. 38 (2020) 1817–1831.
[10] A.L. Chen, N. Shang, Y. Ouyang, et al., eScience 2 (2022) 192–200.
[11] X.D. Wang, Y. Bai, X.R. Wang, C. Wu, Chin. J. Chem. 38 (2020) 1847–1869.
[12] Y.F. Su, J.Y. Zhao, L. Chen, et al., Chin. J. Chem. 39 (2021) 402–420.
[13] Z.Y. Shen, W.D. Zhang, G.N. Zhu, et al., Small Methods 4 (2019) 1900592.
[14] O.W. Sheng, J.H. Zheng, Z.J. Ju, et al., Adv. Mater. 32 (2020) 2000223.
[15] X. Li, Z.H. Ren, M.N. Banis, et al., ACS Energy Lett. 4 (2019) 2480–2488.
[16] D. Aurbach, E.E. Yair, O. Chusid, et al., J. Electrochem. Soc. 141 (1994) 603–611.
[17] D. Aurbach, B.M. Markovs, A. Shechter, E.E. Yair, J. Electrochem. Soc. 143 (1996) 3809–3820.
[18] D. Aurbach, J. Power Sources 89 (2000) 206–218.
[19] G. Vardar, W.J. Bowman, Q. Lu, et al., Chem. Mater. 30 (2018) 6259–6276.
[20] H.J. Guo, H.X. Wang, Y.J. Liu, et al., J. Am. Chem. Soc. 142 (2020) 20752–20762.
[21] H. Marceau, C.S. Kim, A. Paolella, et al., J. Power Sources 319 (2016) 247–254.
[22] Z.Z. Yang, Z.Y. Zhu, J. Ma, et al., Adv. Energy Mater. 6 (2016) 1600806.
[23] E. Peled, D. Golodnitsky, G. Ardel, J. Electrochem. Soc. 144 (1997) 208–209.
[24] J. Christensen, J. Newman, J. Electrochem. Soc. 151 (2004) 1977–1988.
[25] S.Q. Shi, P. Lu, Z.Y. Liu, et al., J. Am. Chem. Soc. 134 (2012) 15476–15487.
[26] O. Borodin, G.V. Zhuang, P.N. Ross, K. Xu, J. Phys. Chem. C 117 (2013) 7433–7444.
[27] X.X. Ma, X. Shen, X. Chen, et al., Small Struct. 3 (2022) 2200071.
[28] J.H. Cui, L.C. Meng, S. Jiang, Phys. Chem. Chem. Phys. 24 (2022) 27355–27361.
[29] Y.B. Xu, H.P. Wu, Y. He, et al., Nano Lett. 20 (2020) 418–425.
[30] B. Han, Z. Zhang, Y.C. Zou, et al., Adv. Mater. 33 (2021) 2100404.
[31] O. Borodin, G.D. Smith, P. Fan, J. Phys. Chem. B 110 (2006) 22773–22779.
[32] B. Takeshi, K. Sodeyama, K. Yoshiumi, T. Yoshitaka, Phys. Chem. Chem. Phys. 22 (2020) 10764–10774.
[33] O. Borodin, D. Bedrov, J. Phys. Chem. C 118 (2014) 18362–18371.
[34] N. Yao, X. Chen, Z.H. Fu, Q. Zhang, Chem. Rev. 122 (2022) 10970–11021.
[35] E. Paled, J. Electrochem. Soc. 126 (1979) 2047–2051.
[36] G. Kresse, J. Furthmiiller, Comput. Mater. Sci. 6 (1996) 15–50.
[37] K. Xu, Chem. Rev. 114 (2014) 11503–11618.
[38] P.E. Blöchl, Phys. Rev. B 50 (1994) 17953–17979.
[39] S. Grimme, J. Comput. Chem. 27 (2006) 1787–1799.
[40] M. Parrinello, A. Rahman, J. Appl. Phys. 52 (1981) 7182–7190.
[41] M. Parrinello, A. Rahman, Phys. Rev. Lett. 45 (1980) 1196–1199.
[42] S. Nosé, J. Chem. Phys. 81 (1984) 511–519.
[43] W.G. Hoover, Phys. Rev. A 31 (1985) 1695–1697.
[44] J.Y. Liang, X.D. Zhang, X.X. Zeng, et al., Angew. Chem. Int. Ed. 59 (2020) 6585–6589.
[45] L. Martinez, R. Andrade, E.G. Birgin, J.M. Martinez, J. Comput. Chem. 30 (2009) 2157–2164.
[46] R. Gomer, Rep. Prog. Phys. 53 (1990) 917–1002.
[47] S.P. Ong, Y. Mo, W.D. Richards, et al., Energy Environ. Sci. 6 (2013) 148–156.
[48] T.H. Gao, W. Lu, Electrochim. Acta 323 (2019) 134791.
[49] X.F. He, Y. Zhu, A. Epstein, Y.F. Mo, Npj Comput. Mater. 4 (2018) 18–27.
[50] T.P. Hu, J.X. Tian, F.Z. Dai, et al., J. Am. Chem. Soc. 145 (2023) 1327–1333.
[51] H. Duan, W.P. Chen, M. Fan, et al., Angew. Chem. Int. Ed. 59 (2020) 12069–12075.